Journal of Environmental Radioactivity 195 (2018) 60–66

Contents lists available at ScienceDirect

Journal of Environmental Radioactivity

journal homepage: www.elsevier.com/locate/jenvrad

Detection of radon with biosensors based on the lead(II)-induced conformational change of aptamer HTG and malachite green fluorescence probe

Shiya Li, Hongwen Liu, Guiying Yang, Shimeng Liu, Ran Liu, Changyin Lv*

College of Public Health, University of South China, Hengyang, 421001, China

ARTICLE INFO

Keywords:
Radon
Lead
Fluorescence detection
Radiation damage
Environmental monitoring

ABSTRACT

The aim of this paper is to assemble a new biosensor for detecting the accumulated radon dose in the environment to achieve rapid monitor of radon. Based on the correlation between radon and its stable decay daughter ^{210}Pb, a biosensor using the lead-induced specific aptamer HTG conformational changes, and the organic dye malachite green (MG) as a fluorescent probe was assembled. In these studies, we explored a novel, sensitive, label-free, fluorescence biosensing method for the detection of both radon and lead. The fluorescence intensity difference has a linear relationship with Pb^{2+} and the accumulated radon concentration from 6.87×10^3 Bq·h/m^3 to 3.49×10^5 Bq·h/m^3. The lead and radon detection limits of this method are 6.7 nmol/L and 2.06×10^3 Bq·h/m^3, respectively. The student's t-test results indicated that the new method was reliable and stable. The detection method is sensitive, accurate, easy to operate, has a wide linear range and is highly selective. In the sampling and determination processes of radon, the radiation harm to human health can be effectively avoided.

1. Introduction

Radon is a colourless, tasteless, odourless, radioactive inert gas, which is known as an “invisible killer”. Radon includes three isotopes of ^{222}Rn, ^{220}Rn, and ^{219}Rn, which are derived from the uranium series, thorium series and actinides, respectively. The common, hazardous radon refers to the ^{222}Rn isotope (having a half-life of 3.825 years) is generated from a long-life radionuclide Ra($T_{1/2}$ = 1600a) in the uranium series. After the decay, a series of nuclides are produced, and the stable isotope ^{210}Pb is formed as the final step(Cheng, 2008). Radon exists in rocks and soil under buildings, decorative marble, water sources, natural gas and coal combustion products, etc(Noh et al., 2016; Chang, 2002). The harm to human health from radon radiation accounts for more than 55% of the total radiation harm in one's life(Zhang et al., 2011). Radon has a high penetration performance, can be intercepted by the respiratory system and is deposited in the lungs (Torres-Durán et al., 2014, Giri and Pant, 2018). Hence, radon and its decay daughters are believed to be the second leading risk factor for lung cancer. The WHO ranks radon as one of the nineteen environmental carcinogens(IPCS, 1999), and the international cancer organization (IARC) designates radon as a first class carcinogenic factor (USEPA, 2016). Additionally, radon and its decay daughters can penetrate the respiratory mucosa and the blood-air barrier and spread through different body tissues, resulting in radiation harm to organs and blood. In particular, radon can be accumulated in the fat cells of bone marrow for a long time, causing α and β radiation harm to haematopoietic stem cells(Zhang et al., 2011). Consequently, skin cancer, leukaemia, functional damage to the central nervous system, and oesophageal cancer can develop(Salgado-Espinosa et al., 2015). With the development of the nuclear industry, the probability of nuclear accidents has increased, making the public pay more attention to the detection and monitoring of radioactive substances, such as radon. Therefore, it is of great significance to determine the concentration of radon in the environment.

In the decay process, radon radiates alpha- and beta-rays. Typically, physical methods based on the intensity of radiation and chemical methods based on the response of reagents to radiation are applied to detect radon. However, the physical methods are ineffective to detect the cumulative radiation amount, and the chemical methods are ineffective to detect radon at low concentrations. The traditional physical methods are divided into three categories: instant sampling methods (Ding et al., 2009) such as the double-filter film method(Wu et al., 2011), the scintillation method(Liu and Li, 2011), the balloon method (Zhu et al., 2014) and the activated carbon adsorption methods(Fu and

* Corresponding author.
E-mail address: lchy1955@163.com (C. Lv).

https://doi.org/10.1016/j.jenvrad.2018.09.021
Received 20 April 2018; Received in revised form 3 August 2018; Accepted 22 September 2018

Liu, 2007); cumulative sampling methods such as the activated carbon spectroscopy(Wang et al., 2015) and the solid track method(Zhao et al., 2008); and continuous measurement methods such as the electrostatic-collection-type continuous radon monitor(Song et al., 2002). These methods have a series of limitations including expensive instruments, high detection cost, harm to human health, low sensitivity, many interference factors, and so forth. To date, some new radon determination approaches have been developed, such as gas chromatography, photometric analysis, electrochemical analysis, Monte Carlo computer simulation, and others. These methods have new features, but it is still necessary and challengeable to improve existing radon detection technologies in the field of new analytical methods research.

Lead is a common environmental contaminant(Zhang et al., 2012). In recent years, the nucleic acid adaptation theory for lead detection has been well developed. An aptamer biosensor employs aptamer to specifically recognize target molecules and produce response signals. Combining the selectivity of aptamers to target molecules with traditional instrumental analysis methods has allowed for the emergence of new biochemical detection methods(Meng et al., 2016; Saidur et al., 2017). Compared to traditional antibodies, aptamers have the advantages of simple synthesis in vitro, low cost, no animal or cellular experiments, high thermal stability, high affinity, high specificity, and low toxicity(Wu and Kwon, 2016). Resulting from electrostatic interactions, hydrogen bonding, stacking effects, and shape matching between the aptamer and target molecule, the aptamer will form a specific secondary structure from a random coiling state into a stable spatial structure(Debnath et al., 2017). This change can be verified from the circular dichroism spectra (CD spectra)(Zhang et al., 2008). The affinity to organic dye is related to the type of spatial structure, and the changes in the response signals are related with the analyte concentration (Nguyen et al., 2017).

Based on the decay of ^{222}Rn to produce lead, we proposed a new label-free fluorescence biosensing method to detect radon based on its decay daughter lead(Deng et al., 2016; Long et al., 2016). The lead ions induce the aptamer T30695 to form a stable G-quadruplex, and hence, the single strand T30695 can no longer form a double helix structure with its complementary strand. Therefore, the positively charged fluorescent dye PG could not insert itself into the double strand plane and the minor groove of the double helix, producing a weaker fluorescence. Meanwhile, the fluorescent dye PG is added, and the single-strand T30695, which not affected by the lead ions, is combined with its complementary strand to form a double helix structure, producing a strong fluorescence.

Malachite green (MG) is a green crystalline triphenylmethane dye with a metallic lustre. Bhasikuttan et al. (2007) found that the interaction between malachite green and the G-quadruplex could produce fluorescence. Kong et al. (2009) believed that crystal violet could distinguish the anti-parallel and parallel structures in the G-quadruplex, and triphenylmethane dyes could serve as the fluorescence probe for the detection of G-quadruplex. Guo et al. (2009) showed that the energy transfer fluorescence spectroscopy of malachite green could identify the intramolecular and intermolecular G-quadruplex and identify single- and double-strand DNA. Ryoko et al.(Uda et al., 2017) reported that malachite green could preferentially combine with G-quadruplex in the form of terminal stacking or in situ insertion, and the combination could produce a strong fluorescence.

Based on the specific recognition ability of the aptamer and the fluorescence produced by the combination of malachite green and the anti-parallel G-quadruplex, we constructed a new fluorescence biosensor platform to detect radon and its decay daughter, lead.

2. Materials and methods

2.1. Equipment and reagents

This study was conducted in a radon chamber at the Sixth Research Institute of Nuclear Industry. The radon concentration was determined using a RAD7 electronic radon detector (Durridge, USA). The experiments utilized a Thermo Fisher Lumina fluorescence spectrophotometer (Thermo Fisher Scientific Incorporation, USA) with a scanning speed of 1200 nm/min. The slits for excitation and emission wavelengths were 10 nm and 10 nm, respectively. We also used a circular dichroism JASCO-815 instrument (JASCO Corporation, Japan) with a scanning speed of 100 nm/min and scanning range of 230–350 nm.

PAGE-purified oligonucleotide: HTG (5′-AGGGTTAGGGTTAGGGTTAGGG-3′) diluted with ultrapure water to a concentration of 100 μM was stored at 4 °C. The organic dye malachite green was diluted with ultrapure water to a concentration of 0.5 mM and stored at 4 °C. The standard lead solution used was diluted with ultrapure water to a concentration of 100 mg/L of Pb^{2+} in the working solution. Trisaminomethane (Tris) with a purity of at least 99.9% was used to form a Tris-HAc buffer for the radon samples and a pH of 6.5. All reagents were diluted with ultrapure water with a resistivity of 18.25 MΩ cm.

2.2. Sampling method of the decay daughter lead

10 mL of 0.2% acetic acid was placed in a petri dish, which was then covered with a mixed-cellulose microporous membrane to prohibit airborne lead-containing pollutants into the petri dish. The schematic diagram of chemical sampling radon is shown in Fig. 1. In addition, sampling times of 2, 4, 8, 12, 20, 24, 42, 60, 72 and 84 h were set. The petri dish was placed in the radon chamber for accumulative irradiation, and the lid was removed. Then, the petri dish was placed at room temperature for more than three and a half days, which is longer than the half-life of radon. The decay daughter lead was absorbed with the dilute acetic acid and was converted to lead ions. After the sampling process, the sample was diluted with the 0.2% acetic acid until the total volume reached 10 mL. The details of operating standard are shown in Table S1(See Supplementary material).

2.3. Fluorescence detection method for standard Pb^{2+} solutions

Two-millilitre EP tubes were used to contain 5 mM of Tris-HAc (trisaminomethane-acetic acid buffer solution, pH = 6.5), a certain amount of standard Pb^{2+} solution, and 0.6 μM of aptamer HTG. After incubation at 37 °C for 90 min, 3.0 μM of malachite green was added, and the total volume was increased using ultra-pure water to 200 μL. The incubation of these sample solutions continued for another 10 min. Meanwhile, the corresponding control group was prepared. The fluorescence intensity F values of the sample solutions and F_0 values of the blank solutions identified an excitation wavelength of 645 nm and an emission wavelength of 680 nm. Then, the fluorescence intensity difference was calculated as $\Delta F = F - F_0$.

2.4. Fluorescence detection method for samples after radon radiation

Likewise, the decay daughter lead was absorbed with 0.2% acetic

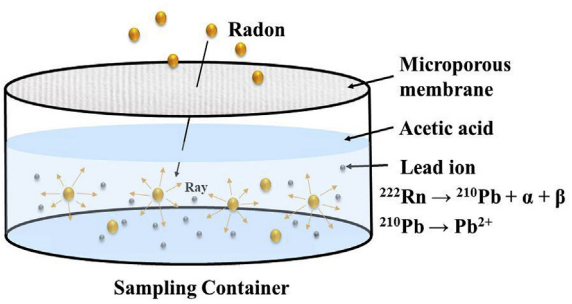

Fig. 1. Schematic diagram of chemical sampling radon.

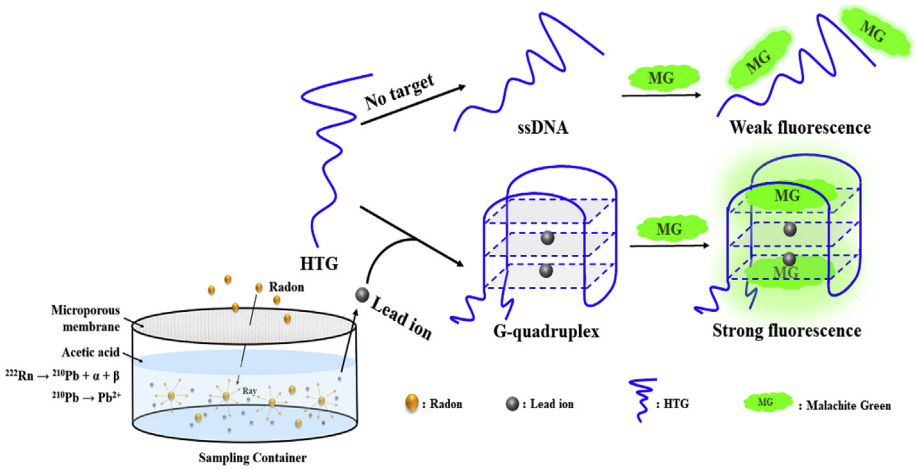

Fig. 2. Schematic diagram of Pb^{2+}-induced conformational changes of HTG.

acid, and 0.2% acetic acid was used as the control group. Moreover, 50 μL of the sample solution was treated following the procedure shown in the section "Fluorescence detection method for standard Pb^{2+} solutions" for the determination of the fluorescence intensity.

3. Results

3.1. Principles of the experiment

The guanine-rich single oligonucleotide HTG is a specific aptamer. In the absence of target molecules, free HTG is in a random coiling state. The negatively charged phosphate backbone of the single-strand DNA interacts with malachite green through electrostatic interactions, producing a weak fluorescence (F_0). The Pb^{2+} can induce the conformational change in the HTG to form a stable anti-parallel G-quadruplex. With the addition of malachite green, the Pb^{2+} moves to the centre of the G-quadruplex, and the positively charged benzene ring of MG interacts with the plane of the G-quadruplex via π-stacking, forming a stable rigid structure and producing a strong fluorescence (F).The schematic diagram is shown in Fig. 2.

With the increase in the Pb^{2+} concentration, the amount of G-quadruplex formed from the increase of induction, increasing the fluorescence intensity of the system. In a certain range of Pb^{2+}, the change of the fluorescence intensity (ΔF) has a linear relationship with the Pb^{2+} concentration. As such, the Pb^{2+} concentration in the solution can be calculated from the ΔF.

After the decay, radon is converted into the daughter lead:

$$^{222}Rn \rightarrow {}^{210}Pb + \alpha + \beta$$

The lead is dissolved in 0.2% acetic acid and converted into cations, triggering the above-stated "HTG–MG" switch and forming the fluorescence biosensor. The higher the radon concentration in the air is, the higher the Pb^{2+} concentration in the solution is, and the greater the ΔF value is. To determine the ΔF value, the cumulative radon radiation quantity will be indirectly measured. Based on the conformational transformation of the HTG induced by Pb^{2+} and the different fluorescence responses of MG to DNA with different conformations, a label-free sensitive radon detection method is developed in the present work.

3.2. Validation of the principles

To verify the correctness of the principles, we measured the fluorescence intensity of the MG, HTG + MG, and Pb^{2+} + HTG + MG in this study, as shown in Fig. 3. The MG system itself had nearly no fluorescence. The single-strand HTG was in a random coiling state without pairing base groups. The electrostatic interaction between the MG and

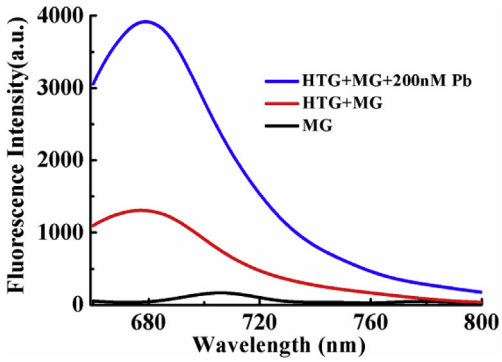

Fig. 3. Fluorescence emission spectra of MG in Tris–HAc (5 mM, pH 6.5) buffer solution under different conditions. The concentrations of HTG, Pb^{2+} and MG were 0.6 μM, 200 nM and 3.0 μM, respectively.

single-strand HTG was weak, and the fluorescence intensity of the "HTG + MG" system was correspondingly very weak. After the addition of Pb^{2+} on the guanine-rich single-strand HTG, the fluorescence intensity of the "Pb^{2+} + HTG + MG" system increased significantly, indicating that lead ions induced the conformational change in the HTG and formed the G-quadruplex. The combination of the organic dye MG and the G-quadruplex produced a strong fluorescence. After the lead standard solution was replaced with a radon-containing sample, similar phenomena were observed.

Moreover, the CD spectra of the HTG, HTG + MG, HTG + Pb^{2+} and HTG + Pb^{2+} + MG systems were measured in this study, as shown in

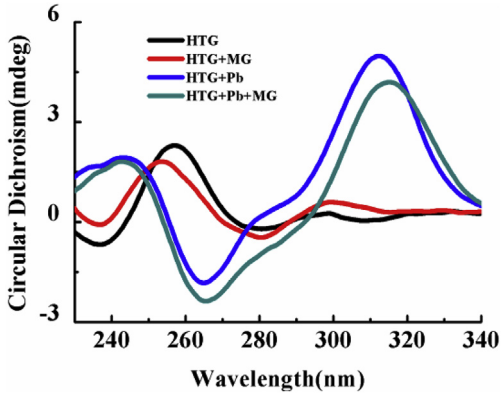

Fig. 4. Circular dichroism spectra of 9 μM aptamer and 45 μM MG in the presence and absence of 14 μM Pb^{2+}.

Fig. 4. The spectrum of single-strand HTG exhibits a positive signal at 256 nm and negative signals at 238 nm and 280 nm. These signals are assigned to the base stacking resulting from the random coiling state of single-strand DNA in a solution, consistent with the reported(Zhang et al., 2008) results of single-strand DNA: 5′-$(TAGGG)_4$-3′. With the addition of the Pb^{2+}, positive signals at 240 nm and 312 nm and a negative signal at 262 nm were observed. These results indicate that the Pb^{2+} reacted with HTG and induced the conformational change in the HTG to form an anti-parallel G-quadruplex.

In the presence of 200 nM Pb^{2+}, the "Pb^{2+} + HTG + MG" system exhibits strong fluorescence. With the additional presence of 2 μM EDTA, the EDTA will be coordinated with Pb^{2+}, forming a stable Pb^{2+}–EDTA complex and lowering the Pb^{2+} concentration in the solution. Consequently, the formation of the G-quadruplex and the combination of the MG and G-quadruplex will be hindered, leading to a decrease in the fluorescence intensity of the system. In the experiments, the fluorescence spectra of the "Pb^{2+} + EDTA + HTG + MG," "HTG + MG + EDTA," and "HTG + MG" systems were similar in shape and fluorescence intensity, implying that the change in the fluorescence intensity was dependent on the concentration of Pb^{2+}. After the lead standard solutions were replaced with real samples, the fluorescence spectra showed similar phenomena. These experimental results evidence those principles proposed above. The experimental results are shown in Fig. 5.

3.3. Optimization of the operational parameters for radon detection

The conditions of our research were influenced by a variety of factors. Therefore, we optimized the operating parameters for radon detection to ensure the formation of the G-quadruplex and its combination with malachite green.

In the correlative study of aptamers, the Tris-HAc buffer system is often chosen to control the acidity and alkalinity of the solution. Accordingly, we employed a Tris-HAc buffer solution to regulate the pH. Fig. S1 (See Supplementary material) indicates that the Δ*F* value gradually increased when the pH increased to 6.5. Then, the ΔF value gradually decreased when the pH was higher than 6.5. The possible reasons are that Pb^{2+} will be hydrolysed to form $Pb(OH)_2$ precipitates in a high alkali solution or that malachite green will be protonated, and the solubility of the oligonucleotide will decrease in a high acidic solution. Thus, the Tris-HAc buffer at a pH of 6.5 was selected as the optimal reaction condition. At this condition, the formation of the Pb^{2+}-induced G-quadruplex was greatly favoured, and thus, the fluorescence intensity produced by the combination of the MG and G-quadruplex was the highest.

To maintain the stability of the reaction system, we optimized the concentration of the Tris-HAc buffer system. From Fig. S2 (See Supplementary material), we can see that the Δ*F* value reached a maximum when the buffer concentrations increased to 5 mM. With the increase in the Tris-HAc buffer concentration, the buffer capacity of the system increased, and the pH of the system was more stable, which was favourable to the formation of the G-quadruplex. Therefore, the fluorescence intensity difference increased. In view of these results, 20 μL of 50 mM of the Tris-HAc buffer solution should be added to the reaction system.

The concentration of the aptamer HTG has a relatively large influence on the formation of the G-quadruplex. Fig. S3 (See Supplementary material) indicates that the ΔF value increased with the increase of the HTG concentration in the range of 0.2 μM–0.6 μM. However, when the HTG concentration is over 0.6 μM, the Δ*F* value decreased. Consequently, the following experiments were carried out with an HTG concentration of 0.6 μM.

The concentration of malachite green is directly related to the production of fluorescence. Fig. S4 (See Supplementary material) shows that the Δ*F* value is maximized when the MG concentration reached 3.0 μM. The results indicated that the benzene rings of MG were stacked to form a rigid structure(Guo et al., 2009), making the fluorescence intensity of the control group increase and the Δ*F* value to decrease. Hence, 3.0 μM is an appropriate concentration of the MG for combination with the G-quadruplex.

Due to aptamer sensitivity to the temperature, six representative temperature values of 18, 25 30, 37, 45 and 55 °C were screened in this study, as shown in Fig. S5 (See Supplementary material). At low temperatures, the elastic vibration of malachite green was limited, inhibiting its vibration to eliminate excitation(Guo et al., 2009), increasing the fluorescence intensity of the control group increase. As the temperature increased from 18 °C to 37 °C, the elastic vibration of malachite green was enhanced. However, when the reaction temperature was higher than 37 °C, the hydrolysis of DNA was enhanced, resulting in the decrease in the Δ*F* value. Therefore, the reaction should be conducted at 37 °C.

Based on optimized conditions, we studied the effect of incubation time on the Δ*F* value, including the incubation time of the G-quadruplex formation (Fig. S6A, See Supplementary material), and the incubation time of the G-quadruplex combined with the MG (Fig. S6B, See Supplementary material). Eventually, 90 min and 10 min were chosen as the optimized conditions for the two respective incubation times.

3.4. Influence of impurities

Under the same conditions, we independently studied the influence of the common cations Na^+, Ce^{2+}, Bi^{3+}, Cd^{2+}, Tb^{3+}, Zn^{2+}, Al^{3+}, Cu^{2+}, Ca^{2+}, NH_4^+, K^+, Mg^{2+}, and Mn^{2+} on the determination of Pb^{2+}, as shown in Fig. 6. Among them, only K^+ could reduce the determination sensitivity of the fluorescence system. The above-stated sampling method could prevent the pollution of metal ions, including K^+. Thereby, the interference of metal ions to the measurement of radon is negligible.

The concentration was 200 nmol/L for Pb^{2+}; 20 μmol/L for Na^+,

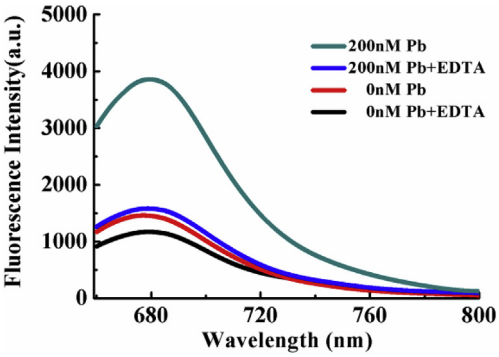

Fig. 5. Fluorescence emission spectra under different conditions. c_{HTG} = 600 nM, c_{Pb} = 200 nM, c_{MG} = 3 μM, Tris-HAc = 5 mM, pH = 6.5.

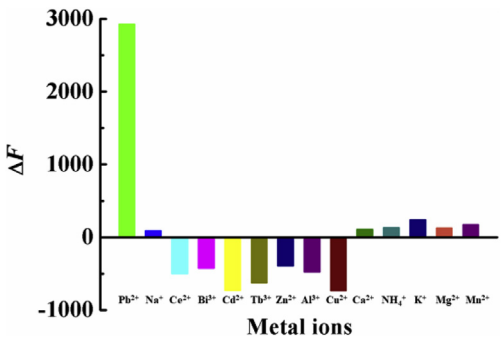

Fig. 6. Selectivity of the HTG-MG biosensor for Pb^{2+} over other competing metal ions.

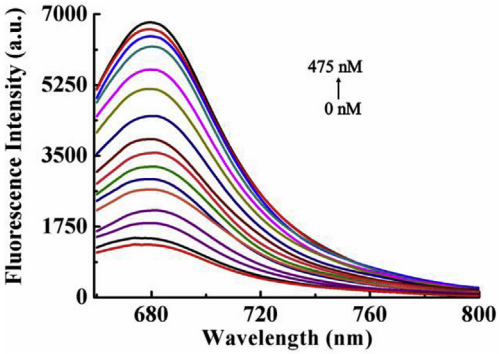

Fig. 7. Fluorescence emission spectra of the sensing system on exposure to: 0, 25, 50, 75, 100, 125, 150, 175, 200,250 ,300 ,350 ,400 ,425 ,450 and 475 nmol/L Pb^{2+}.

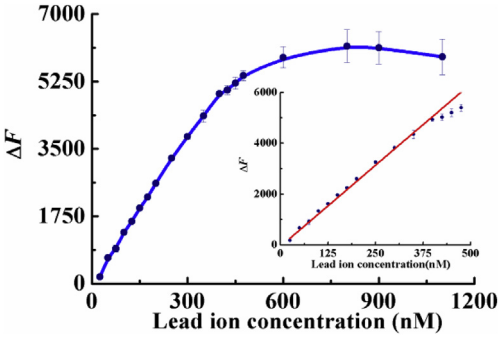

Fig. 8. Relationship of lead ion concentration and fluorescence intensity.

Ce^{2+}, Bi^{3+}, Cd^{2+}, Tb^{3+}, Zn^{2+}, Al^{3+}, Cu^{2+}; 4 μmol/L for Ca^{2+}, NH_4^+;400 nmol/L for K^+, Mn^{2+};2 μmol/L for Mg^{2+}.

3.5. Calibration curve, detection limit and precision for lead determination

Under optimized conditions, a series of Pb^{2+} standard solutions were prepared to determine the fluorescence intensity at 645 nm. The fluorescence intensity increased gradually in the Pb^{2+} concentration range of 0–600 nmol/L. When the Pb^{2+} concentration was over 475 nmol/L, the increase of the fluorescence intensity was significantly reduced. From Fig. 7 and Fig. 8, we can see that the Pb^{2+} concentration in the range of 22.4 nmol/L to 475 nmol/L, the ΔF value had a good linear relationship with the Pb^{2+} concentration, and the regression equation was $\Delta F = 12.7989c_{Pb}$-60.979 (r = 0.9964). A blank solution was measured 11 times to that determine the detection limit of Pb^{2+} was 6.7 nmol/L following the equation $C_L = 3s_b/k$. The standard solutions containing 100 nmol/L, 250 nmol/L, and 450 nmol/L of Pb^{2+} were measured 11 times, and the relative standard deviations were 2.45%, 1.74%, and 3.00%, respectively. Compared with the other methods for measuring Pb^{2+} and radon as shown in Table 1 and Table 2, this method has the advantages of a low detection limit and a wide linear range.

Table 2
Comparison with other methods for the determine of Radon concentration.

Methods	Signal Probe	Target	LOD (× 10^3Bq·h/m^3)	Reference
Wireless sensing	PMMA film/ SSNTs	Radon	20.30	Du et al., 2011
Track etching	Polycarbonate film (CR-39)	Radon	2.10	GB/T 14582－1993
Flu	HTG/MG	Radon	2.06	This Work

'Flu' refer to Fluorescence; 'PMMA film' refer to polymethyl methacrylate film; 'SSNTs' refer to solid state nuclear tracks.

3.6. Quantitative determination and modelling of the cumulative radon concentration

Using the sampling method, the radon radiation sample solutions with concentrations of 1.09, 2.05, 4.19,5.89, 10.08, 12.04, 20.16, 29.87, 34.97, and 40.66 (× 10^4 Bq·h/m^3) were collected at the Sixth Research Institute of Nuclear Industry of the University of South China. Ten radon-containing samples were prepared following the procedure described in section "Sampling method of the decay daughter lead." The determination was carried out six times for each sample according to the procedure described in section 2.4. In addition, the standard addition recovery of three kinds of low, medium and high concentration samples was measured to investigate the precision and accuracy of the determination method.

As shown in Table 3, with the increase in the cumulative radon concentration, the ΔF value and Pb content of the sample increased gradually. From Fig. 9, we can see that when radon concentration was in the range of 6.87 × 10^3 Bq·h/m^3 to 3.49 × 10^5 Bq·h/m^3, the ΔF value had a linear relationship with c_{Pb} and c_{Rn}: $\Delta F = 12.7989c_{Pb}{}^{2+} - 60.979$ (r = 0.9964); and $\Delta F = 7.3718c_{Rn} + 642.66$ (r = 0.9987). As such, a quantitative measurement model correlating the cumulative radon radiation amount with its decay daughter lead could be developed. The detection limit of radon is 2.06 × 10^3 Bq·h/m^3.

3.7. Radon detection methodology comparison

According to the National Occupational Health Standard of the People's Republic of China GBZ/T 210.4–2008 (GBZ/T 210.4－2008) "Guide for establishing occupational health standards－Part 4: Determination methods of air chemicals in workplace", the research method was used to perform six measurements at three concentrations of high, medium and low in the measurement range simultaneously with the published standard methods or recognized classical methods. Using test results for equivalence experiment.

To further test this new method, six radon samples of different concentrations were collected using the sampling method. Each sample was measured in parallel six times (Jin and Xu, 2017). The results of our research were compared with the sample taken using the RAD7 radon monitor, as shown in Table 4. The two methods were compared by the Student's t-test. Within the confidence interval of 95%, the statistical analysis results showed that $t_1 = 1.22$, $t_2 = 1.27$, $t_3 = 1.04$, $t_4 = 0.83$,

Table 1
Comparison with other methods to determine the Pb^{2+} concentration.

Methods	Signal Probe	Target	LOD (nM)	Linear Range	Reference
ODR	PS2.M	Pb^{2+}	100.0	500nM–10μM	Ma et al., 2018
Col	PS2.M/ABTS	Pb^{2+}	32.0	100nM-10μM	Li et al., 2010
Flu	FAM-TBA/AuNPs	Pb^{2+}	10.0	12.5–100 nM	Liu and Huang, 2014.
Raman	RhG- $Au_{core}Ag_{shell}$NP-ssDNA	Pb^{2+}	7.0	50–700 nM	Liu et al., 2014
Flu	HTG/MG	Pb^{2+}	6.7	22.4–475 nM	This Work

'ODR' refer to optical darkness ratio; 'Flu' refer to Fluorescence; 'Col' refer to colorimetry; 'FAM' refer to carboxyfluorescein; 'RhG' refer to rhodamine 6G; 'ABTS' refer to 2,2′-azino-bis (3-ethylbenzothiazoline-6-sulfonic acid) diammonium salt.

Table 3
Determination results of Pb^{2+} in the samples (n = 6).

Sample	c_{Rn} (Bq·h/m^3)	ΔF (a.u.)	Found (× 10^{-7} mol/L)	Added (× 10^{-7} mol/L)	Total found (× 10^{-7} mol/L)	RSD (%)	Recovery (%)
1	1.09 × 10^4	680.00	0.58	1.00	1.60	3.12	104.45
2	20.2 × 10^4	2212.77	1.78	1.00	2.78	1.44	100.15
3	29.8 × 10^4	2790.54	2.26	1.00	3.18	4.63	96.48

'Found' and 'Added' refer to the final concentration.

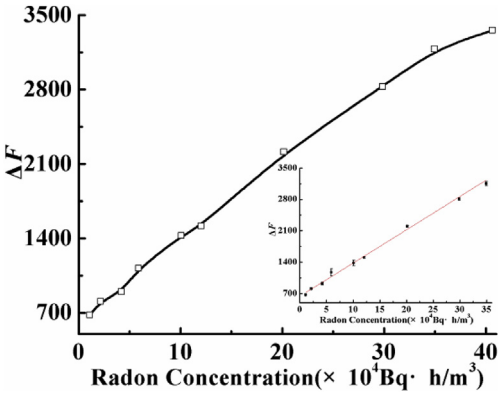

Fig. 9. Correlation curve of fluorescence intensity and radon concentration.

Table 4
Determination results of radon in the samples (n = 6).

Sample	Method	Found (× 10^{4}Bq·h/m^3)	SD (× 10^{4}Bq·h/m^3)	RSD (%)	*t*-test
1	TW	2.19	0.06	2.75	1.22
	RAD7	2.15	0.04	1.70	
2	TW	5.19	0.20	3.81	1.27
	RAD7	5.07	0.10	2.01	
3	TW	10.44	0.31	2.94	1.04
	RAD7	10.29	0.15	1.45	
4	TW	20.82	0.47	2.24	0.83
	RAD7	21.01	0.33	1.57	
5	TW	29.49	0.85	2.88	0.86
	RAD7	29.82	0.40	1.35	
6	TW	33.36	0.99	2.97	0.88
	RAD7	33.78	0.65	1.93	

Theoretical $t_{0.05/2,10}$ = 2.228; 'TW' refer to this work; 'Found' refer to mean value of six measurements.

t_5 = 0.86 and t_6 = 0.88. Compared with the theoretical value of $t_{0.05/2,10}$ = 2.228, we accepted H_0 according to the level α = 0.05; i.e., the difference between the two methods was not statistically significant. The statistical analysis shown that the new method results are consistent with those obtained from the RAD7 radon monitor. The new method is stable and reliable.

4. Conclusions

The conformational change in the aptamer HTG was induced by lead ions, resulting in the formation of the G-quadruplex with a basket-type anti-parallel structure. The G-quadruplex combined with the MG to produce a strong fluorescence. These are the principles of the new lead ion detection system with high sensitivity and high selectivity.

In the radiation field, acetic acid was employed to capture the radioactive radon. After the absorption of the decay daughter lead with 0.2% acetic acid, the formed lead ions would trigger the HTG–MG fluorescence "switch" in this determination system. The relationship between the cumulative radon radiation amount and the fluorescence intensity change of the system was established. Namely, a label-free fluorescent biosensor for the determination of radon was assembled. The experimental results determined by this approach are consistent with the data obtained from the RAD7 physical detection method.

The radon-containing samples were collected with a vessel sealed with a mixed-cellulose microporous membrane. This vessel has the following advantages: firstly, the radon can be smoothly introduced into the sampler and solution for complete adsorption of the decay daughter lead; secondly, other radioactive gases, as impurities, can also be introduced but cannot be converted into lead and has no influence on the radon determination; and thirdly, the particulates in the air can be blocked before they enter the acetic acid solution, excluding the influence of lead, potassium and other metal ions on the determination.

The "Pb^{2+}-HTG-MG" label-free fluorescent biosensor can be utilized to detect lead and radon, and the detection limits of lead and radon are 6.7 nmol/L and 2.06 × 10^{3}Bq·h/m^3, respectively. Compared with other similar former works, this new method has a wider linear range to detect both radon and lead. This detection method is applicable to the determination of lead in water, air, and food. More importantly, it is fast and simple in the determination of radon and does not have the drawbacks of physical detection methods, including radiation damage, environmental temperature interference, and humidity interference. This method has a low detection limit, short sampling time, wider linear range and high accuracy.

Conflicts of interest

The authors declare that they have no conflict of interest.

Acknowledgments

Funding: This work was supported by the National Natural Science Foundation of China [grant numbers 81473021].

Appendix A. Supplementary data

Supplementary data to this article can be found online at https://doi.org/10.1016/j.jenvrad.2018.09.021.

References

Bhasikuttan, A.,C., Mohanty, J., Pal, H., 2007. Interaction of malachite green with guanine-rich single-stranded DNA: preferential binding to a G-quadruplex. Angew. Chem. Int. Ed. 46, 9305–9307. https://doi.org/10.1002/anie.200703251.
Chang, G.,L., 2002. Radon and its hazards. Uranium Geol. 18, 122–128.
Cheng, Y.,X., 2008. Hazard and control measures of radon and its progenies in the environment. Geoscience 22, 857–868.
Debnath, M., Ghosh, S., Chauhan, A., Paul, R., Bhattacharyy, K., Dash, J., 2017. Preferential targeting of I-motifs and G-quadruplexes by small molecules. Chem. Sci. 8, 7448–7456. https://doi.org/10.1039/C7SC02693E.
Deng, H., Long, M., Tian, G., Song, C., Liu, H., Hu, L., Lv, C., 2016. Detection of radon based on the lead-induced conformational change in aptamer T30695. RSC Adv. 6, 37254–37257. https://doi.org/10.1039/c6ra03481k.
Ding, W.,C., Fang, F., Ruan, J.,H., Wang, M., Huang, Q., 2009. A new method for consecutive measurement of air radon. Nucl. Tech. 32, 545–549.
Du, N., Liao, L., Xiao, Y., Xiao, X., Zhao, Z., Lin, Y., 2011. Determination of radon using solid state nuclear tracks wireless sensing method. Anal. Chim. Acta 686, 121–125.
Fu, P.,F., Liu, S.,S., 2007. Measurement of indoor radon consistence in Beijing buildings with activated carbon box method. J. Beijing Union Univ.(Nat. Sci.) 21, 70–72. https://doi.org/10.16255/j_.cnki_.ldxbz.2007.02.018.
GB/T 14582－1993, 1993. Standard Methods for Radon Measurement in Environmental

Air. National Standards of the People's Republic of China.
GBZ/T 210.4 – 2008, 2008. Guide for establishing occupational health standards – Part 4: determination methods of air chemicals in workplace. In: National Occupational Health Standards of the People's Republic of China.
Giri, A., Pant, D., 2018. Inhalation dose due to Rn-222, Rn-220 and their progeny in indoor environments. Appl. Radiat. Isot. 132, 116–121. https://doi.org/10.1016/j.apradiso.2017.11.027.
Guo, J.,.H., Zhu, L.,N., Kong, D.,M., Shen, H.,X., 2009. Triphenylmethane dyes as fluorescent probes for G-quadruplex recognition. Talanta 80, 607–613. https://doi.org/10.1016/j.talanta.2009.07.034.
IPCS (International Programme on Chemical Safety), 1999. Enviromental Health Criteria 211.Health effects of interactions between tobecoo use and exposure to other agents. Genewa: World Health Organization (WHO) 57–59.
Jin, J., Xu, H., 2017. Determination of cadmium and chromium in food by inductively coupled plasma atomic emission spectrometry after incomplete digestion. Chin. J. Health Lab. Technol. 27, 3068–3070.
Kong, D.,M., Ma, Y.,E., Wu, J., Shen, H.,X., 2009. Discrimination of G-quadruplexes from duplex and single-stranded DNAs with fluorescence and energy-transfer fluorescence spectra of crystal violet. Chem. Eur J. 15, 901–909. https://doi.org/10.1002/chem.200801441.
Li, T., Wang, E., Dong, S., 2010. Lead(II)-Induced allosteric G-quadruplex DNAzyme as a colorimetric and chemiluminescence sensor for highly sensitive and selective Pb^{2+} detection. Anal. Chem. 82, 151–1520.
Liu, C., Huang, C.Z., 2014. Detection of lead ions in water based on the surface energy transfer between gold nanoparticles and fluorescent dyes. Chin. J. Anal. Chem. 42, 1195–1198. https://doi.org/10.1016/s1872-2040(14)60760-x.
Liu, Y.,N., Li, Y.,Z., 2011. Scintillation flask method for measuring radon in the high voltage power. HUNAN Agri. Machinery 38, 47–49.
Liu, Q., Wei, Y., Luo, Y., Liang, A., Jiang, Z., 2014. Quantitative analysis of trace Pb(II) by a DNAzyme cracking-rhodamine 6G SERRS probe on Au(core)Ag(shell) nanosol substrate. Spectrochim. Acta A. 128, 806–811. https://doi.org/10.1016/j.saa.2014.03.008.
Long, M., Deng, H., Tian, G., Song, C., Liu, H., Shen, Y., Lv, C., 2016. A novel detection of radon based on its decay product inducing conformational changes of an aptamer probe. Anal. Chim. Acta 936, 202–207. https://doi.org/10.1016/j.aca.2016.06.025.
Ma, L.,H., Wang, H.,B., Fang, B.Y., Tan, F., Cao, Y.,C., Zhao, Y.,D., 2018. Visual detection of trace lead ion based on aptamer and silver staining nano-metal composite. Colloids Surf., B 162, 415–419. https://doi.org/10.1016/j.colsurfb.2017.12.011.
Meng, H.,M., Liu, H., Kuai, H., Peng, R., Mo, L., Zhang, X.,B., 2016. Aptamer-integrated DNA nanostructures for biosensing, bioimaging and cancer therapy. Chem. Soc. Rev. 45, 2583–2602. https://doi.org/10.1039/c5cs00645g.
Nguyen, V.,T., Kwon, Y.,S., Gu, M.B., 2017. Aptamer-based environmental biosensors for small molecule contaminants. Curr. Opin. Biotechnol. 45, 15–23. https://doi.org/10.1016/j.copbio.2016.11.020.
Noh, J., Sohn, J., Cho, J., Kang, D.,R., Joo, S., Kim, C., Shin, D.C., 2016. Residential radon and environmental burden of disease among Non-smokers. Ann. Occup. Environ. Med. 28. https://doi.org/10.1186/s40557-016-0092-5.
Saidur, M.,R., Aziz, A.,R., Basirun, W.,J., 2017. Recent advances in DNA-based electrochemical biosensors for heavy metal ion detection: a review. Biosens. Bioelectron. 90, 125–139. https://doi.org/10.1016/j.bios.2016.11.039.
Salgado-Espinosa, T., Barros-Dios, J.,M., Ruano-Ravina, A., 2015. Radon exposure and oropharyngeal cancer risk. Cancer Lett. 369, 45–49. https://doi.org/10.1016/j.canlet.2015.08.025.
Song, G., Zhang, B.,Y., Gong, J.,P., 2002. The influence of relative humidity on the check result of the electrostatic collecting type of continuum radon measurement apparatus. Bull. China Soc. Mineral Petrol. Geochem. 21, 58–60.
Torres-Durán, M., Barros-Dios, J.,M., Fernández-Villar, A., Ruano-Ravina, A., 2014. Residential radon and lung cancer in never smokers. A systematic review. Cancer Lett. 345, 21–26. https://doi.org/10.1016/j.canlet.2013.12.010.
Uda, R.M., Matsui, T., Takei, M., 2017. Binding of malachite green promotes stability and shows preference for a human telomere DNA G-quadruplex. Supramol. Chem. 29, 553–560. https://doi.org/10.1080/10610278.2017.1297447.
USEPA (U.S. Environmental Protection Agency), 2016. A citizen's guide to radon: the guide to protecting yourself and your family from radon. Indoor Air Quality(IAQ) 2–15.
Wang, X., Zhang, X.,J., Wang, H.,L., Liu, H.,F., 2015. CO2 movement monitoring after CO2 injection in coal seam based on radon measurement. Saf. Coal Mine 46, 133–136. https://doi.org/10.13347/j.cnki.mkaq.2015.03.040.
Wu, Y.,X., Kwon, Y.,J., 2016. Aptamers: the “evolution” of SELEX. Methods 106, 21–28. https://doi.org/10.1016/j.ymeth.2016.04.020.
Wu, H.,X., Liu, Y.,J., Yang, B., Qiu, G.,X., Liu, Q.,C., 2011. Evaluation of dose arising from 222Rn, decay products of 222Rn and 220Rn to staff from a certain nuclear power plant. Nucl. Power Eng. 32, 122–126.
Zhang, H.,J., Wang, X.,F., Wang, P., Ai, X.,C., Zhang, J.P., 2008. Spectroscopic study on the binding of a cationic porphyrin to DNA G-quadruplex under different K^+ concentrations. Photochem. Photobiol. Sci. 7, 948. https://doi.org/10.1039/b809322a.
Zhang, S.,F., Li, X.,L., Sun, Q.,F., 2011. Health hazard effects of radon and its daughters. Chin. Prev. M ed. 12, 726–732. https://doi.org/10.16506/j_.1009-6639.2011.08.028.
Zhang, X., Yang, L., Li, Y., Li, H., Wang, W., Ye, B., 2012. Impacts of lead-zinc mining and smelting on the enviromental and human health in China. Environ. Monit. Assess. 184, 2261–2273. https://doi.org/10.1007/s10661-011-2115-6.
Zhao, Y.,L., Fang, F., Lv, M., 2008. Indoor radon detection and protection. J. Environ. Health 25, 72–73. https://doi.org/10.16241/j.cnki.1001-5914.2008.01.005.
Zhu, G., Ge, L., Li, Z., 2014. Application of the instrument measuring radon in balloon method to evaluating indoor radon concentration. Nucl. Tech. 37, 1–5. https://doi.org/10.11889/j.0253-3219.2014.hjs.37.080201.